Review

Review of RoCoF Estimation Techniques for Low-Inertia Power Systems

Xiaoyu Deng [1], Ruo Mo [1], Pengliang Wang [1], Junru Chen [1], Dongliang Nan [2] and Muyang Liu [1,*

[1] School of Electrical Engineering, Xinjiang University, Urumqi 830046, China; xyd@stu.xju.edu.cn (X.D.)
[2] Electric Power Research Institute, State Grid Xinjiang Electric Power Co., Ltd., Urumqi 830011, China
* Correspondence: muyang.liu@xju.edu.cn; Tel.: +86-13677352908

Abstract: As the traditional generation is gradually replaced by inverter-based resources, a lack of rotational inertia is now a common issue of modern power systems, which leads to an increasingly larger rate of change of frequency (RoCoF) following contingencies and may result in frequency collapse. As a crucial index of the frequency security and stability of power systems, the accurate estimation of the RoCoF can be a foundation for the development of advanced operations and control techniques of the future power system. This paper firstly analyzes the role of the RoCoF in typical blackouts occurring in recent years and discusses the physical and numerical nature of the RoCoF; then, by introducing the frequency spatial distribution of the power system, the paper discusses the concept of the "center" RoCoF that can present the frequency security and stability of the entire system. The estimation and prediction techniques of the maximal power system RoCoF following a contingency and the existing real-time tracking techniques of the power system RoCoF are comprehensively reviewed. Finally, the open questions and related research topics of the RoCoF estimation are discussed.

Keywords: frequency stability; rate of change of frequency (RoCoF); power system stability; phasor measurement unit (PMU)

1. Introduction

1.1. Motivation and Background

With the goal to decrease carbon emissions, inverter-based resources (IBRs) including wind and solar generation and energy storage systems play increasingly important roles in modern power systems around the world [1,2]. With the increasingly high penetration of IBRs, a lack of rotational inertia gradually becomes a common issue for power systems [3,4]. One of the significant results is the decreasing frequency stability of power systems. The operating frequency of low-inertia IBR-leading systems is vulnerable to any disturbance; the rate of change of frequency (RoCoF) will rapidly increase following a contingency, which leads to large frequency deviations and even the cascading failure of the system [5–7].

Severe blackouts occurring in recent years are typical extreme results for unexpected large RoCoFs following a contingency, e.g., the "8.9" blackout in Britain in 2019 [8]. In this context, the maximal RoCoF during the frequency evaluation of a power system has become a key index to indicate the frequency security of power systems [9,10], which can be used to evaluate the security margin for the potential risk to trigger the unexpected frequency protections that can lead to the cascading failure of the system. In modern power systems, the node frequency is obtained by local measurement; the corresponding RoCoF, therefore, is also local [11,12]. For an interconnected large power system, the long electrical distances among the nodes and the uneven inertia distribution lead to complicated spatial features of dynamic frequency. It means that the local RoCoF can be improper for use as the index of the frequency security of the entire system, as it can be at a significantly different level [13]. In this context, it is important to find a "center" RoCoF that can present the stability and security features of the entire system.

With a clear definition of the power system RoCoF that indicates the frequency security of the entire power system, newly developed artificial intelligence (AI) techniques have been applied to predict the maximal RoCoF following the potential contingencies of a system based on historical operating datum [14,15].

Meanwhile, faced with increasing frequency security and stability challenges for power systems, modern control strategies of IBRs have been developed to provide inertia and frequency support to the grid. To achieve the fast frequency response, RoCoF tends to be used as one of the input signals for these modern control techniques, e.g., virtual inertia control [16,17]. Moreover, RoCoF can feed to the newly developed protections, e.g., RoCoF relay [18,19]. Therefore, to ensure the smooth operating of the modern controllers and protections fed by the RoCoF signal, accurate real-time RoCoF tracking is crucial. Considering the mathematical nature of RoCoF, namely, a rate of change of a time-variant variable, RoCoF cannot be directly measured but needs to be computed by the internal algorithm of measuring devices for the real-time variables of AC systems. The most common measurement device that allows to track the RoCoF is the synchrophasor [20]. The accuracy and robustness against the measurement noise of the obtained RoCoF highly depend on the estimation techniques. At present, discrete Fourier transform (DFT) is still the most widely used phasor estimation technique [21–23]. However, the accuracy of this technique is still questionable, especially when phase jump issues occur [24,25]. To further increase the accuracy and reliability of RoCoF tracking, correlation phasor algorithms have been developed in recent years, which can be roughly divided into the following three categories: DFT-based methods, Kalman filter techniques, and other methods.

1.2. Contribution

This paper aims to provide a comprehensive review of RoCoF estimation techniques for power systems including related concepts and estimation techniques. The specific contributions of the paper are the following:

(i) Discussion on the role of the RoCoF in power system cascading failure and understanding the power system RoCoF;

(ii) Review the estimation and prediction techniques of the maximal RoCoF following a contingency;

(iii) Review the different methods of RoCoF real-time tracking techniques with a discussion on the advantages and disadvantages as well as the further development of existing methods.

1.3. Oriagnization

The rest of this paper is organized as follows. Section 2 discusses the typical blackouts occurring in recent years, explains the physical and numerical characteristics of power system RoCoF, and introduces the concept of "center" RoCoF. In Section 3, the estimation and prediction techniques of the maximal RoCoF following a contingency are reviewed, and a power system with zero rotational inertia is discussed in depth. Section 4 reviews the existing RoCoF real-time tracking techniques. The conclusions and related future research topics are provided in Section 5.

2. Frequency Stability of the Low-Inertia Power System

This section firstly discusses the typical blackouts in recent years that resulted from a lack of inertia and especially analyzes the features of the RoCoF during the dynamic evaluation of the blackouts, and then explains the "role" of the inertia and RoCoF in modern power systems. On this basis, the concept of "center" RoCoF is introduced. Table 1 lists the nomenclature of parameters in Section 2.

Table 1. Section 2 nomenclature.

Variable	Description
H_{eq}, H_G, H_V	Equivalent inertia constant of the power system, synchronous generator and IBRs
f^0, f_{CoI}, f	Normal frequency, frequency of center of inertia, and inner frequency of the sources
ΔP_G	The change of the output power from the generations providing the frequency support to the system
ΔP_L	The unbalanced active power caused by the contingency
D	The damping factor of the power system
S	The rated power
N_G, N_V	The number of synchronous machines and IBRs
$\mathbf{f}_B$	The vector consisting of the node frequency of the power system
$\mathbf{f}_G$	The vector consisting of the equivalent speed of the generation set
$\mathbf{A}$	The parameter matrix of the power system
$\overline{\mathbf{Y}}$	The admittance matrix of the power system
$\mathbf{h}$	Normalized inertia constants with dimension $m \times 1$
$\mathbf{1}_{n \times 1}, \mathbf{I}_m$	Identity matrix with dimension $n \times 1$ and unit matrix with dimension $m \times m$

2.1. Typical Blackouts in Low-Inertia Systems

The rotational inertia level of the power system continuously decreases alongside the adjustment of the energy composition structure of the power grid [3]. In recent years, frequency collapses caused by a lack of inertia have occurred in many countries, which largely increases attention to the frequency security and stability of modern power systems. Figure 1 summarizes the typical blackouts in low-inertia systems from recent years.
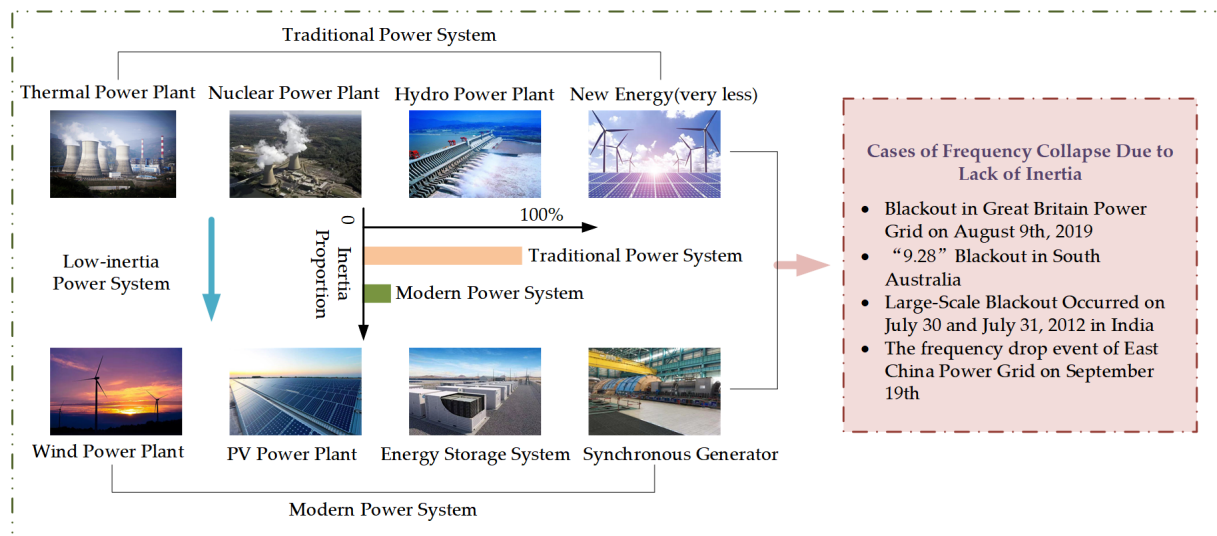
Figure 1. Frequency security problems of low-inertia systems.

The details for each blackout shown in Figure 1 are the following:

(i) British "8.9" blackout: At around 17:00 local time on 9 August 2019, due to a lightning strike, a single-phase grounding short-circuit fault occurred on a transmission line in the British power system and caused the successive disconnection of the Little Barford gas power station and Hornsea offshore wind plant as their frequency protections were triggered. The inertia of the British power system at that time was 210 GW·s [8], for the 30% wind penetration. The RoCoF of the British system was recorded at 500 ms and 0.135 Hz/s following the contingency [8], which is over the threshold of the RoCoF protection of the most distributed sources at 0.125 Hz/s [8,26] and thus led to the extra 345 MW power loss due to the cut-off of the distributed sources. As a result, an under-frequency load shedding (UFLS) of the system was triggered, and finally led to a large-scale power outage in England and Wales. The load loss was about 3.2% of the whole British system and about 1 million people were affected. During this incident, the unexpectedly

large RoCoF resulted in the unexpected trip of the generation units, and therefore, the occurrence of UFLS.

(ii) South Australia "9.28" blackout: On the afternoon of 28 September 2016, local time, a severe typhoon and storm hit South Australia and caused the break of six transmission lines. The voltage drop occurred six times within 2 min at the point of common coupling (PCC) of the wind farm at Davenport, which led to the large-scale cut-off of wind generations and resulted in the loss of the generation of 445 MW [27]. To maintain the frequency stability of the state system, there was about 850–900 MW of power imported by the Heywood tie line that went beyond its maximal capacity at 600 MW [28]. Finally, the state grid was isolated due to the trip of the Heywood tie line and thus the power supply of the entire state was interrupted for about 50 h. At the time of the accident, the wind and solar power penetration of the South Australia system was 48.36%, and the inertia of the system was 3000 MW·s, the lowest level in history. At the beginning of the accident, the RoCoF reached 6.1 Hz/s and the frequency nadir was 47 Hz, i.e., −3 Hz below the nominal value [27–29].

(iii) India "7.30" and "7.31" blackouts: On 30–31 July 2012, the largest power outage occurred in India since 2000, which affected 20 Indian states and more than 600 million residents. The normal frequency of the Indian power system is 49.5~50.2 Hz [30], which allows for relatively large frequency fluctuations compared with the other countries with strong power systems. On the day the blackout occurred, 47 transmission lines above 400 kV were out of work for maintenance, which further weakened the grid. At the beginning of this event, the 220 kV transmission line Gwalior–Malanpur I tripped, which led to a cascading failure including the disconnection between the western and northern India power systems. The northern India power system collapsed after 25 s of the disconnection. On the following day, the Rajasthan State generation unit tripped and was followed by the trip of the 220 kV Badod Modak line [30,31]. After 2 min, the disconnection of the western and eastern Indian power system occurred, which was followed by the collapse of the eastern and northern systems. The total installed capacity of the Indian power grid was 202,979 MW, and the renewable energy penetration rate of the system was 33.66% [31,32]. The typical low-inertia features resulted in a large RoCoF following the contingency and thus led to the above two cascading failures. Frequency deviations over 1.2 Hz were observed during the blackout [32].

According to the above discussion, a relatively low-inertia level and extremely high RoCoF was recorded during these events. Therefore, the following subsection discusses the "role" of inertia and RoCoF for modern power systems.

2.2. The "Role" of Inertia and RoCoF for Modern Power Systems

Power system frequency stability refers to the power system's ability to maintain a stable frequency following a large disturbance that leads to the unbalance between the power supply and load demand [3,33]. The collapse of the frequency stability observed in typical blackouts is discussed in the above subsection. For a power system that maintains the frequency stability following a contingency, its frequency evolution trajectory is shown in Figure 2, which can be divided into four stages [34,35]: inertia response, primary frequency control (PFC), secondary frequency control (SFC), and tertiary frequency control (TFC).

As we can see in Figure 2, at the first stage of the evolution, the frequency drops following the contingency. At this stage, the inertial response dominates the frequency dynamics by converting the kinetic energy into electrical energy to depress the frequency deviation from the normal value. The larger the inertia, the more the stored kinetic energy is, and therefore, the smaller the RoCoF is at this stage [2,36,37]. When the frequency is out of the dead band of the turbine governor (TG), the TG acts and the PFC is triggered. With the effect of PFC, the frequency starts to recover from the nadir. Note that the stages that are dominated by the inertial response and the PFC can be partly overlapped [34], as shown in the yellow area of Figure 2. There usually exists a quasi-steady status with obvious frequency deviations at the second stage of the frequency evolution due to the limited effect

of PFC. Since then, in the following SFC and TFC dominant stages, the frequency slowly recovers to the normal value with the RoCoF approaching zero.
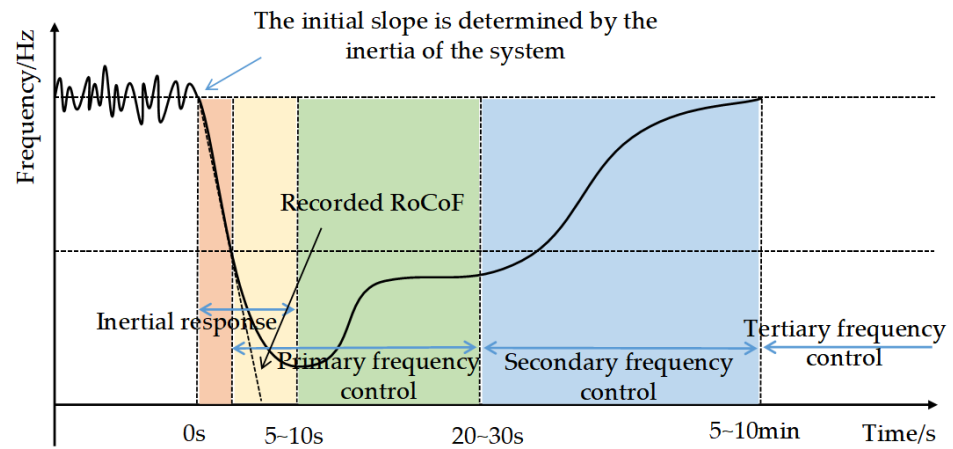

Figure 2. Typical frequency evolution of a power system.

According to the above discussion, the RoCoF estimation for the initial response and PFC-dominant stages is interesting. One can introduce the following equation to describe the relationship between the inertia and RoCoF [34,38]:

$$\frac{2H_{eq}}{f^0}\frac{df_{CoI}}{dt} = \Delta P_G(t) - \Delta P_L - D_{eq}\Delta f \tag{1}$$

where Δf is the frequency deviation from the normal frequency; H_{eq} can be computed by Equation (2):

$$H_{eq} = \frac{\sum\limits_{i=1}^{N_G} H_{G,i}S_i + \sum\limits_{j=1}^{N_V} H_{V,j}S_j}{\sum\limits_{i=1}^{N_G} S_i + \sum\limits_{j=1}^{N_V} S_j} \tag{2}$$

where $H_{G,i}$ is the equivalent inertia constant of the *i*-th synchronous generator; S_i is the rated power of the *i*-th synchronous generator; $H_{V,j}$ is the equivalent inertia constant of the *j*-th IBRs providing virtual inertia to the grid; S_j is the rated power of the *j*-th IBRs. Equation (2) indicates that the inertia of the grid mainly consists of two parts, namely the rotational inertia from synchronous generator and the virtual inertia from IBRs [34]. It is worth noting that $H_{V,j}$ is usually unknown and time-varying because it depends on the operating state and control method of the IBR. The relevant inertia estimation techniques for power systems with high penetrations of IBRs have therefore been developed in recent years [34,39,40], which can be the technical foundation to predict the critical value of the RoCoF of the power system.

With the developing interconnections between regional grids, the modern power system has an increasingly wider geographical distribution. The inertia level of different subsystems can be very different due to the uneven distributions of the synchronous generator with large inertia and the IBR that cannot provide inertia support. In this context, the frequency event occurring at different places within the power system may be followed by the frequency evaluation with very different features, including the RoCoF. Therefore, the distribution of the inertia, to some extent, shapes the temporal and spatial characteristics of the dynamic frequency.

2.3. Concept of "Center" RoCoF

2.3.1. Frequency of CoI and Its Estimation Method

The real-world power system constantly suffers from the disturbances of the stochastics of renewable power and load and can be attacked by unpredictable events such as a

tripped critical transmission line and unexpected loss of generation, which leads to the ever-changing frequency of the system [41]. The dynamic frequency at each node of the power system is under the impact of many factors [38,42], e.g., the local inertia level and distances from the disturbances, and therefore, can be different from each other. Professor F. Milano proposes the following frequency divider formula (FDF) to describe the spatial distribution of the power system frequency [43]:

$$\begin{cases} \mathbf{f}_B = \mathbf{1} + \mathbf{A}(\mathbf{f}_G - \mathbf{1}) \\ \mathbf{A} = -(\mathrm{Im}\{\overline{\mathbf{Y}}_{BB} + \overline{\mathbf{Y}}_{B0}\})^{-1}\mathrm{Im}\{\overline{\mathbf{Y}}_{BG}\} \end{cases} \tag{3}$$

where $\overline{\mathbf{Y}}_{BB}$ is the admittance matrix of power grid; $\overline{\mathbf{Y}}_{B0}$ is a diagonal matrix, which takes into account the internal impedances of synchronous generators at the generator buses; $\overline{\mathbf{Y}}_{BG}$ is the admittance matrix at the bus.

As FDF implies, the dynamic frequency at each node of the power system is different [43,44]. The concept of frequency of center of inertia (CoI) is proposed to present the "center" frequency (also abbreviated as system frequency in some reports and papers) of the power system [38,45–48]:

$$f_{CoI} = \frac{\sum\limits_{i=1}^{N} H_{eq,i} f_i}{\sum\limits_{i=1}^{N} H_{eq,i}} \tag{4}$$

where $H_{eq,i}$ and f_i are the inertia constant and the inner frequency of the i-th sources.

Reference [46] proposes the following expression to estimate the frequency of the CoI:

$$\begin{cases} f_{CoI}^* = \boldsymbol{\xi}^T \mathbf{f}_B + \boldsymbol{\alpha} \\ \boldsymbol{\xi}^T = -\mathbf{h}^T \mathrm{Im}\{\overline{\mathbf{Y}}_{BG}^+\}\mathrm{Im}\{\overline{\mathbf{Y}}_{BB} + \overline{\mathbf{Y}}_{B0}\} \\ \boldsymbol{\alpha} = 1 - \boldsymbol{\xi}^T \mathbf{1}_{n,1} \end{cases} \tag{5}$$

where $\overline{\mathbf{Y}}_{BG}^+$ is the left inverse of $\overline{\mathbf{Y}}_{BG}$, i.e., $\overline{\mathbf{Y}}_{BG}^+ \overline{\mathbf{Y}}_{BG} = \mathbf{I}_m$; the i-th element of $\mathbf{h}$ is $h_i = H_i / H_T$ and $H_T = \sum_{j=1}^{m} H_j$.

2.3.2. RoCoF of the Frequency of CoI

With the concept of frequency of CoI, we can deduce the "center" RoCoF that can present the frequency security feature of the power system as the time derivative of the frequency of CoI. The threshold to trigger the RoCoF protection of the power system in some countries, such as Britain [49] and Denmark [49], has been set as a maximal value of the system RoCoF.

3. Estimation and Prediction of the Maximal RoCoF following a Contingency

According to the above discussion, the maximal RoCoF of the system discussed in this section is derived from the frequency of CoI following a contingency. This section discusses the estimation and prediction of the maximal RoCoF following a contingency. It is worth noting that the maximal RoCoF prediction techniques still need to be improved in accuracy and interpretability. Relevant solutions are provided in this section, mainly using the method of slope estimation. The magnitude of the maximal RoCoF highly depends on the contingency and the inertia level of the system, which is an important index to present the frequency security of the power system [49–51]. This section discusses the estimation of the maximal RoCoF following an already-occurred event and the prediction of the maximal RoCoF following a potential contingency of the system; the specific classification is shown in Figure 3. Table 2 lists the nomenclature of parameters in Section 3.
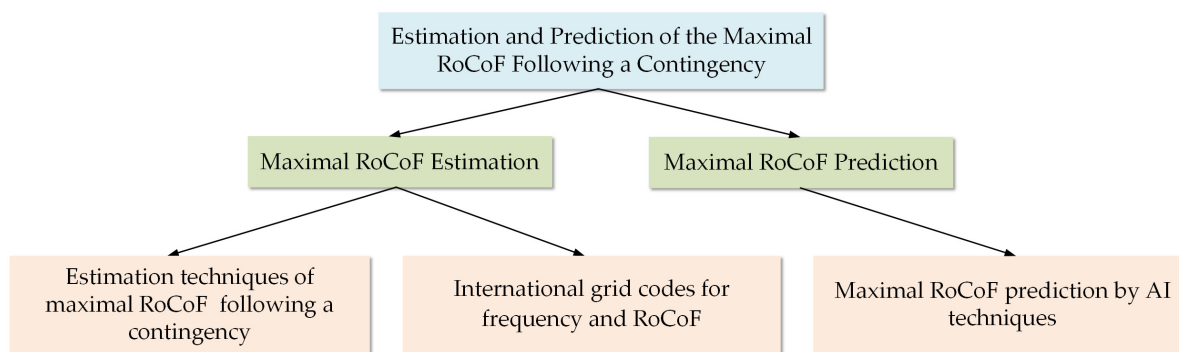
Figure 3. Taxonomy of offline RoCoF estimation techniques for power systems.

Table 2. Section 3 nomenclature.

Variable	Description
$\widetilde{f}$	Averaged system frequency
T	A short period following the contingency
$f(t_0), f(t_0 + T)$	The pre-contingency frequency and the frequency of a short period T following the contingency
RoCoF_m^*	The approximated maximal RoCoF

3.1. Maximal RoCoF Estimation

The most commonly used estimation method of the maximal RoCoF is calculating the maximal RoCoF from the obtained trajectory of the dynamic frequency following an event. This method can provide the most accurate RoCoF to the Transmission System Operators (TSOs). The curve fitting technique used to analyze the maximal power system RoCoF is found in reference [52], where a fifth-order polynomial to mimic the frequency response of the power system is proposed and the "analytic" RoCoF function as the first-time derivative of the polynomial can be obtained. One can easily deduce the maximal RoCoF according to the obtained RoCoF function. Then, reference [53] assumes a polynomial to describe the dynamic frequency $\widetilde{f}$ of the power system:

$$\widetilde{f}(t) = k[1 + \sigma e^{-\varsigma \omega_n t} \sin(\omega_r t + \phi)] \tag{6}$$

where $k, \sigma, \varsigma, \omega_n, \omega_r$, and ϕ are unknown parameters of $\widetilde{f}$ and t is the time, these parameters need to be identified according to the dynamic behavior of the system. Following that work, reference [54] proposes an adaptive polynomial fitting technique to describe the dynamic frequency and also the RoCoF.

During the frequency evolution following a contingency, however, since the completed frequency trajectory is not available, the maximal RoCoF "saw" by the control and operation center (recorded as RoCoF_m^* in the remainder of the paper) of the system is usually the approximated value calculated by the data of the frequency obtained within a very short period following the contingency [35,52–54]:

$$\text{RoCoF}_m^* = \frac{f(t_0 + T) - f(t_0)}{T} \tag{7}$$

where $f(t_0)$ is usually very close to the nominal value. The specific T for different grid codes is listed in Table 3.

Table 3. International grid codes for frequency and RoCoF.

Grid Code	T	Security Threshold (Normal Frequency)
IEEE [55]	N.A.	0.4 Hz/s (60 Hz)
Denmark [49,56]	500 ms	2 Hz/s (50 Hz)
Ireland [49,56]	200 ms	1 Hz/s (50 Hz)
UK [56]	500 ms	1 Hz/s (50 Hz)
Germany [49,56]	500 ms	2 Hz/s (50 Hz)
Australia [49]	N.A.	No standard for RoCoF (50 Hz)
USA [49,57]	N.A.	No standard for RoCoF (60 Hz)

Table 3 shows the typical approximated maximal RoCoF and their corresponding security thresholds from different grid codes [49,55–57]. As we can see in Table 3, the method to define the RoCoF_m^* and its security threshold for several European countries has been issued, while there is no specific rule in the IEEE standards to estimate RoCoF_m^* but a security threshold for the maximal RoCoF is provided. Australian and USA grid codes have not listed a clear requirement for RoCoF yet, but the related discussions become increasingly broad with the increasingly high penetration of the IBRs in these national grids.

The security threshold of a system RoCoF has to be small enough to protect the on-grid devices under extreme scenarios, while it also has to be large enough to avoid triggering unexpected cascading failures. Therefore, the RoCoF threshold in some countries, e.g., the UK and Ireland, has been modified with the developed online devices and increasingly high penetration of IBRs in recent years [49,56]. Ireland increased the RoCoF threshold from 0.5 Hz/s to 1 Hz/s in 2020 [49]. The new settings for RoCoF may be issued with the development and application of virtual inertia techniques.

3.2. Maximal RoCoF Prediction

With the rapid development of AI techniques in recent years, the applications of AI on the stability and security assessment of power systems have become a hot topic [2,14,15]. One of the typical applications of the AI algorithm on power system analysis is predicting the possible behavior of the system via training the proposed algorithm to learn from the historical operation datum. In this context, the AI algorithms that can predict the maximal RoCoF of the potential contingencies of the power system have been proposed.

Reference [14] utilizes a deep learning network based on stacked denoising auto encoders to predict the indexes of the frequency evolutions following the possible large disturbances including the maximal frequency deviation, maximal RoCoF, and quasi-steady-state frequency. Reference [15] proposes an online frequency security assessment method based on the multi-layer extreme learning machine (ML-ELM). In the process of unsupervised training, an automatic encoder algorithm and regularization coefficient are utilized to optimize layer by layer, which can accurately predict the maximal RoCoF with a relatively small computational burden.

Although AI techniques are supposed to have a wide application for power system analysis, in the current phase, the lack of interpretability raises a common doubt for their further development in the power system field [39]. A reliable and accurate maximal RoCoF prediction AI technique that can actually assist the TSO with satisfied interpretability may be still on the way.

3.3. Towards the Power System with Zero Rotational Inertia

To date, 100% renewable energy systems have been built and can operate safely and stably for a long time. For example, many countries have built or are close to building 100% renewable energy power systems, including hydro, wind, and solar power sources [1,3,58,59]. The hydropower included in renewable energy power systems can provide rotational inertia to the grid, and at the same time, these kinds of power systems are always equipped with synchronous compensators to improve the voltage stability of the power system, which

can also provide rotational inertia [1,3]. Therefore, the 100% renewable energy system can be regarded as a low-inertia power system rather than a zero rotational inertia system.

At present, Xinjiang, China, as the energy base of China, has built a typical ultra-high proportion new energy power system, including 100% new energy areas with only solar, wind power, and energy storage devices, but it has not reached the situation with zero rotational inertia, because there is still asynchronous motors existing in the load side, providing a small amount of inertia support. Theoretically speaking, if there is no asynchronous motor at all on the load side, then the system can be regarded as zero inertia, and since the load side is also 100% power electronic equipment, then this system no longer needs to maintain a 50/60 Hz nominal frequency, because all equipment is connected to the power system via power electronic converters, and even a pure DC system can be formed. However, this kind of system does not exist at present because most of the electrical equipment is designed to operate normally at the nominal frequency. Even if the power supply is 100% power electronization, the system still operates around the nominal frequency in order to satisfy the requirement of most power consumption devices. In this context, to avoid damaging the load-side electrical equipment, the frequency security and stability needs to be ensured by inertial support that depress the frequency fluctuations and extremely high RoCoF [3].

Based on the above discussion, it is necessary to use virtual inertia techniques to provide inertia support to suppress the drastic changes in frequency and RoCoF in all the real-world power systems now and in the near future [60,61]. Considering that virtual inertia is uncertain compared with the constant rotational inertia, because virtual inertia is a typical control technique of the power electronic converters, the effect of the control can be easily affected by the adjustable parameters and the state of the energy sources [60–62]. Therefore, it will become more challenging to set a reasonable RoCoF security threshold and potential RoCoF prediction techniques in the power system with virtual inertia as the main inertial support form due to the high uncertainty of the spatial and temporal distribution of the virtual inertia.

4. Real-Time RoCoF Tracking Techniques

According to the well-known frequency definition of AC power system given in IEEE Std. IEC/IEEE 60255-118-1 [63], the RoCoF can be presented as

$$\text{RoCoF} = \dot{f}(t) = \frac{1}{2\pi}\ddot{\vartheta}(t) = \frac{1}{2\pi}\ddot{\theta}(t) \tag{8}$$

where ϑ is the angular position of the signal $x(t) = X_m(t)\cos(\vartheta(t))$ [63]; θ is the phase difference between the angular position ϑ of the signal x(t) and the phase caused by the reference normal frequency. Equation (8) implies that the measurement device that can track the dynamic voltage/current phase at a node of the power system, namely the synchrophasor, can be used to track the real-time local RoCoF with a proper algorithm; however, RoCoF estimation techniques face great challenges in accuracy and robustness. This section provides a comprehensive review of the existing real-time RoCoF tracking algorithms of synchrophasors, which can be divided into three main categories: (i) DFT-based [64–76], (ii) Kalman filter techniques [77–92], and (iii) other methods [93–100]. The details for each category are provided in the subsection. The specifics are shown in Figure 4. Table 4 lists the nomenclature of parameters in Section 4.
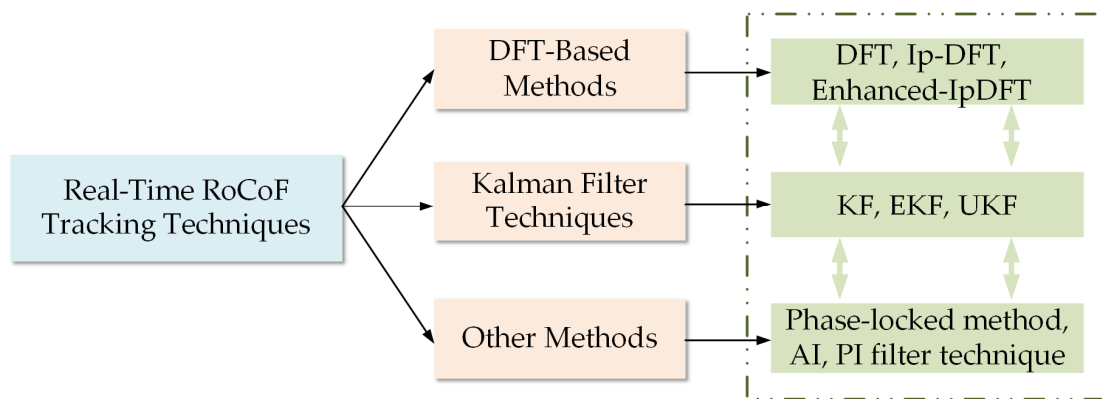
Figure 4. Taxonomy of real-time RoCoF tracking techniques.

Table 4. Section 4 nomenclature.

Variable	Description
V_m	The magnitude of the voltage waveforms
f	The signal frequency to be estimated
ϕ_V	The phase angle
T_s	The sampling interval
f_s	The sampling frequency
x	The vector of state variables
z	The vector of measurements
u	The control vector
A	The state transition matrix
B	The control matrix
H	The measurement matrix
w	The column vector of process noise
v	The column vector of measurement noise
$\hat{\Box}$	Estimated values
$\Box^-$	Predicted values
$\Box^T$	Transposition of the matrix
P	Covariance matrix
Q	Covariance of process noise
K	Kalman gain matrix
R	Covariance of measurement noise
$L, \lambda, \alpha, \kappa, \beta$	Adjustable parameters of UKF algorithm
f, **h**	Vectors consisting of nonlinear state transition functions and measurement functions
$\mathbf{W}^{(m)}, \mathbf{W}^{(c)}$	Weights for the mean and covariance, respectively
K_p, K_i, T_f	PI filter parameters

4.1. DFT-Based Methods

DFT is the most basic and common signal processing method at present. The DFT method can be used to calculate the amplitude phase angle, frequency, and RoCoF of the input signals collected by synchrophasors [64–68]. The voltage/current waveform of the AC power system measured by the synchrophasor can be described as the following:

$$V(t) = V_m \cos(2\pi f t + \phi_V) \tag{9}$$

DFT refers to transforming a discrete time series with finite length into a signal in frequency domain, by sampling the signal at given intervals. For a periodic signal, N points are sampled in each T period, namely, $T = NT_s$. The voltage signal in the frequency domain obtained via DFT is given by

$$V(k) = \sum_{n=0}^{N-1} V(n)e^{-j\frac{2\pi}{N}nk}, k = 0, 1, 2 \ldots N-1 \tag{10}$$

where k is the frequency bin index, n is the sample index.

The dynamic frequency of the system can be estimated by finding the frequency bin index k that corresponds to the largest magnitude in the frequency domain (recorded as k_m). The highest frequency bin represents the fundamental waveform of the signal and its frequency can be the coarse estimation as follows [69]:

$$f_c = k_m \frac{f_s}{N} \tag{11}$$

Because of the spectral leakage and fence effect in sampling, DFT may introduce obvious errors for the processing of signals with relative rapid variations [69–71]. In this context, the improved DFT methods with higher accuracy and robustness against the sampling techniques are developed for real-time RoCoF tracking in the power system.

Reference [71] proposes a windowed DFT which allows the tracking of frequency deviation under various power system operation conditions and RoCoF and presents the satisfied accuracy defined by the IEEE standards.

The interpolated DFT (IpDFT) is another well-known technique, which estimates the synchrophasors by interpolating the DFT spectrum of the signal [72]. The windowed interpolation techniques are used to suppress the spectral leakage of DFT methods via introducing an appropriate window function for sampling. The interpolated DFT can be represented mathematically as follows:

$$V(k) = \sum_{n=0}^{N-1} V(n) e^{-j\frac{2\pi}{N} n(k+\Delta k)}, k = 0, 1, 2 \dots N - 1 \tag{12}$$

where Δk is the interpolation factor and the selection of Δk is related to the window function. In particular, the IpDFT applying windowing function to reduce the spectral leakage effects [66,72,73]. References [67,72,74,75] prove that with proper window function, the IpDFT can largely reduce the errors resulting from the spectral leakage. The Hanning window is better than the traditional rectangular window, with a reduced leakage and fluctuation for IpDFT.

Reference [72] proposes an enhanced IpDFT algorithm for synchronous phasor frequency estimation that computes RoCoF as the first-time derivative of the obtained frequency passing by a low-pass filter. The enhanced IpDFT algorithm combines three different methods to reduce the influence of errors caused by spectrum interference, including windowing, DFT interpolation, and iterative solution [76].

4.2. Kalman Filter Techniques

The Kalman filter technique is widely used in the field of the power system state estimation [77–79]. The real-time RoCoF tracking techniques based on the Kalman filter can effectively avoid the impact of harmonics and noise of the input signal fed into the synchrophasor through solving the optimal estimation problem of the continuous prediction–correction operation [78,80,81]. Kalman filter techniques require the establishment of appropriate state equations and measurement equations that can be solved iteratively; the basic formulas of the standard Kalman filter are shown in (13)–(15) [82,83].

The state/measurement equations of the Kalman filter are

$$\begin{cases} \mathbf{x}_k = \mathbf{A}\mathbf{x}_{k-1} + \mathbf{B}\mathbf{u}_{k-1} + \mathbf{w}_{k-1} \\ \mathbf{z}_k = \mathbf{H}\mathbf{x}_k + \mathbf{v}_k \end{cases} \tag{13}$$

where the subscript k represents the k-th iteration.

The prediction steps of the equations are

$$\begin{cases} \hat{\mathbf{x}}_k^- = \mathbf{A}\hat{\mathbf{x}}_{k-1} + \mathbf{B}\mathbf{u}_{k-1} \\ \mathbf{P}_k^- = \mathbf{A}\mathbf{P}_{k-1}\mathbf{A}^T + \mathbf{Q} \end{cases} \tag{14}$$

The update steps of the equations are

$$\begin{cases} \mathbf{K}_k = \mathbf{P}_k^- \mathbf{H}^T (\mathbf{H}\mathbf{P}_k^- \mathbf{H}^T + \mathbf{R})^{-1} \\ \hat{\mathbf{x}}_k = \hat{\mathbf{x}}_k^- + \mathbf{K}_k (\mathbf{z}_k - \mathbf{H}\hat{\mathbf{x}}_k^-) \\ \quad \mathbf{P}_k = (\mathbf{I} - \mathbf{K}_k \mathbf{H})\mathbf{P}_k^- \end{cases} \tag{15}$$

Reference [83] proposes a method based on the standard Kalman filter in solving the frequency and RoCoF as the state variables, the estimation error of the obtained RoCoF is below 0.1 Hz/s. Reference [84] uses the wavelet-based signal pre-processing technique to remove the noise of the frequency obtained through the wide-area measurement system and then estimates the corresponding RoCoF through a Kalman filter technique similar to the method proposed in [83]. Reference [82] proposes a method based on the Smoothed Taylor–Kalman filter (STKF) technique to track the RoCoF; this method is a linear system based on the Taylor series expansion and the Kalman filter. By using the backward filter based on the smoother, the accuracy of STKF on tracking the frequency and RoCoF is much improved compared with the classic Kalman filter.

References [24,25] show that phase jumps of the input signal resulting from faults can lead to an erroneous frequency and RoCoF estimation. To deal with this issue, the Extended Kalman filter (EKF) and Unscented Kalman filter (UKF) techniques are used for the frequency and RoCoF estimation of the power system. UKF always shows a higher accuracy and better numerical stability than EKF by introducing the unscented transformation (UT) technique to replace the linearization step of EKF [85]. The UKF, therefore, is the most advanced Kalman filter technique for the power system frequency and RoCoF estimation at present. The basic steps of the UKF algorithm are presented in Algorithm 1 [85–87].

From the basic equation of UKF shown in Algorithm 1, it can be found that UKF is consistent with the basic Kalman filter algorithm, including prediction step and update step; UKF, based on UT, abandons the traditional method of linearizing nonlinear functions, and uses UT to deal with the nonlinear transfer of mean and covariance, which becomes the UKF algorithm. It is worth noting that in the process of selecting sigma points, three parameters are very important [88,89]: α determines the distribution state of sigma points, usually $0 \leq \alpha \leq 1$; the specific value of κ depends on the situation, for the case of Gaussian distribution, when the state variable is univariate, $\kappa = 2$ is selected, and when it is multivariate, $\kappa = 3 - L$ is generally used to determine the value of κ; the parameter to be adjusted, β, can improve the accuracy of variance. For Gaussian distribution, $\beta = 2$ is the optimal value.

Reference [90] proposes an algorithm of interpolated DFT combined with UKF, which estimates the frequency and corresponding RoCoF in two steps: firstly, the frequency through the IDFT with the Hanning window is tracked; and then, the UKF method is used to observe the system state including RoCoF, and the accuracy meets all IEEE standards for RoCoF estimation. References [87,91,92] show that the computational complexity of the UKF increases dramatically with the larger system size and therefore may not suit the real-world power system.

Several methods to improve the computational efficiency and the numerical stability of the UKF have been developed, which broaden the applications of UKF on the system with high dimension and nonlinearity, including the real-world power system. Reference [87] points out that during the iterations of the UKF algorithm to solve the dynamic states of the power system, the estimation error covariance $\mathbf{P}$ with positive semi-definiteness may not exist. Therefore, the $\sqrt{\mathbf{P}}$ in the unscented transformation stage cannot be computed properly and the iteration would be terminated without an effective result. Reference [87] compares six different methods to cope with this issue, including the 'schol' algorithm, parameter optimization, modifying the covariance matrix (utilized in the step 3 and 6 in Algorithm 1), modifying the predicted covariance matrix (utilized in the step 3 in Algorithm 1), and using the square-root UKF (SR-UKF) form. The results show that the effect of the SR-UKF that introduces the guaranteed positive semi-definite estimation error covariance is the best at avoiding this numerical issue. In the implementation of SR-UKF,

$\sqrt{\mathbf{P}}$ is considered instead of $\mathbf{P}$ to avoid refactorizing $\mathbf{P}$ at each step, and therefore, effectively improves the computational efficiency and numerical stability of the UKF without the loss of any accuracy.

Algorithm 1: Unscented Kalman Filter

---

1. Compute the sigma points:

$\chi_{k-1} = [\hat{\mathbf{x}}_{k-1}, \hat{\mathbf{x}}_{k-1} + \mathbf{E}, \hat{\mathbf{x}}_{k-1} - \mathbf{E}]$
where $\mathbf{E} = \sqrt{(L+\lambda)\mathbf{P}_{k-1}}$
$\chi_k^- = \mathbf{f}(\chi_{k-1})$

2. Predict the state:

$\hat{\mathbf{x}}_k^- = \sum\limits_{i=0}^{2L} \mathbf{W}_i^{(m)} \chi_{i,k}^-$

3. Predict the covariance:

$\mathbf{P}_k^- = \sum\limits_{i=0}^{2L} \mathbf{W}_i^{(c)} [\chi_{i,k}^- - \hat{\mathbf{x}}_k^-][\chi_{i,k}^- - \hat{\mathbf{x}}_k^-]^T + \mathbf{Q}$

where $\begin{cases} \mathbf{W}_0^{(m)} = \lambda/(L+\lambda) \\ \mathbf{W}_0^{(c)} = \lambda/(L+\lambda) + (1-\alpha^2+\beta) \\ \mathbf{W}_i^{(m)} = \mathbf{W}_i^{(c)} = 1/2(L+\lambda) \end{cases}$

4. The propagated sigma points with measurement function:

$\mathbf{Z}_k^- = \mathbf{h}(\chi_{k-1})$

5. The predicted measurement:

$\hat{\mathbf{z}}_k^- = \sum\limits_{i=0}^{2L} \mathbf{W}_i^{(m)} \mathbf{Z}_{i,k}^-$

6. Compute measurement covariance:

$\mathbf{P}_{\mathbf{z}_k \mathbf{z}_k} = \sum\limits_{i=0}^{2L} \mathbf{W}_i^{(c)} [\mathbf{Z}_{i,k}^- - \hat{\mathbf{z}}_k^-][\mathbf{Z}_{i,k}^- - \hat{\mathbf{z}}_k^-]^T + \mathbf{R}$

7. Compute cross-covariance:

$\mathbf{P}_{\mathbf{x}_k \mathbf{z}_k} = \sum\limits_{i=0}^{2L} \mathbf{W}_i^{(c)} [\chi_{i,k}^- - \hat{\mathbf{x}}_k^-][\mathbf{Z}_{i,k}^- - \hat{\mathbf{z}}_k^-]^T$

8. The Kalman Gain:

$\mathbf{K}_k = \mathbf{P}_{\mathbf{x}_k \mathbf{z}_k} \mathbf{P}_{\mathbf{z}_k \mathbf{z}_k}^{-1}$

9. Update the state:

$\hat{\mathbf{x}}_k = \hat{\mathbf{x}}_k^- + \mathbf{K}_k(\mathbf{z}_k - \hat{\mathbf{z}}_k^-)$

10. Update the covariance:

$\mathbf{P}_k = \mathbf{P}_k^- - \mathbf{K}_k \mathbf{P}_{\mathbf{z}_k \mathbf{z}_k} \mathbf{K}_k^T$

4.3. Other Methods

Reference [93] proposes an orthogonal phase-locked method for frequency estimation that is combined with gradient descent algorithm to model the system. This method tracks the rate of change of angular frequency through Equation (16):

$$\dot{\omega} = -\rho_2 A^2 \sin(2\psi) + 2\rho_2 A^2 u(t) \cos(2\psi) \tag{16}$$

where

$$\begin{cases} A = \sqrt{A_s^2 + A_c^2} \\ \psi = \phi + \tan^{-1}\left(\frac{A_c}{A_s}\right) \end{cases} \tag{17}$$

where ρ is the coefficient that the advised value is 0.5; $u(t)$ is the input signal; A_c and A_s obtain the optimal parameters through gradient descent algorithm. This orthogonal phase-locked method can accurately track the dynamic frequency and the corresponding RoCoF with high robustness against the measurement noise and harmonics. In reference [94], the power system frequency and RoCoF are obtained by computing the space vector (SV) in a reference frame that rotates at the rated angular frequency. Based on [94], reference [95] proposes a digital phase-locked loop to improve the accuracy of the SV-based RoCoF estimation algorithm, by constructing the instantaneous position of a rotating reference frame.

Reference [96] proposes a least square method based on polynomial curve fitting to improve the robustness of RoCoF calculation. Reference [97] designs an accurate RoCoF

estimation algorithm combining DFT and least squares method, which solves the inevitable RoCoF estimation error caused by noise and disturbance in the real frequency measurement through ingenious design. In addition, before using the algorithm, a median filter is designed and applied, and the window size of the algorithm is determined by analyzing the historical event data. Simulation results show that the accuracy of this method in frequency estimation is far less than that of the IEEE standard (the maximum frequency error is 0.005 Hz), and the online/offline RoCoF estimation is compared and analyzed with a time window of 0.3 s, with high accuracy. Reference [98] proposes the generalized Taylor weighted least squares (GTWLS) method to track the power system RoCoF. GTWLS is an extension of the classical Taylor weighted least squares method, which deduces the real-time RoCoF as a function of the real-time frequency deviation. To further improve the accuracy of the RoCoF estimation, reference [98] also suggests to combine the GTWLS with the IpDFT algorithm.

Reference [99] proposes an inflection point detector technique, which only uses the locally measured frequency to estimate the CoI RoCoF and does not mandate PMUs at all generator terminals. This method skillfully uses the second derivative of frequency to change the characteristics of its symbol. The local frequency curve intersects the CoI frequency curve around the inflection points of the former. By connecting the inflection points, we can obtain the approximate estimated value of the CoI frequency, so that the CoI RoCoF can be obtained, accordingly. Reference [100] proposes that the CoI frequency and RoCoF of the power system can be calculated more accurately by PMU data from multiple locations. Firstly, the equivalent inertia constant is obtained by the least squares method, and then the CoI frequency is calculated according to Equation (4), and the RoCoF is the first-time derivative of CoI frequency; the simulation results show that the error can be effectively reduced.

Reference [34] proposes a universal and lightweight PI filter technique; through the output RoCoP of the units, the internal angular frequency of the power supply can be estimated only by the deviation between the bus angular frequency measured by PMU and the rated angular frequency. Then, RoCoF can be obtained by using the first derivative of the internal angular frequency of the power supply output by the PI filter. The control block diagram of the PI filter is shown in Figure 5, and reference [34] suggests that the PI filter with parameters $K_p = 50$, $K_i = 1$, and $T_f = 0.0001$ can effectively track the local RoCoF for inertia estimation.
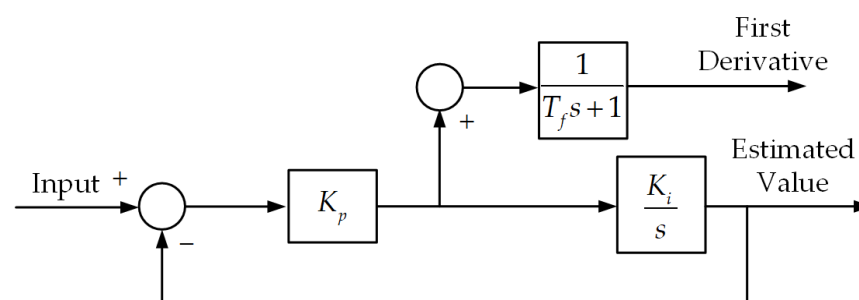

Figure 5. The control block diagram of the PI filter.

4.4. Discussions

Generally speaking, DFT is the most common signal processing method for the existing synchrophasors utilized in power systems. However, the accuracy of real-time RoCoF tracking with DFT can be very sensitive to the noise and sampling techniques. Improved DFT methods, e.g., IpDFT, can improve the accuracy of the frequency and RoCoF estimation. Kalman filter techniques are of great interest for the future development of the power system RoCoF estimation due to its high accuracy and robustness against noise and harmonics. Especially, the improved UKF technique has been proven to be feasible and reliable for the power system state estimation. The heavy computational burden, however, still limits the application of Kalman filter techniques on the real-time RoCoF tracking of the

real-world power system. The RoCoF estimation combining the DFT with the Kalman filter can further improve computational efficiency and accuracy. In addition to the above two kinds of techniques, new methods for phase lock, e.g., orthogonal phase-locked method and digital phase-locked loop, have also been developed to track power system frequency and RoCoF. In addition, new methods of combining the least squares method with other estimation techniques, such as the combination of DFT and least squares method, and GTWLS techniques, have made good progress in RoCoF estimation, are also considered to further improve the accuracy and robustness of the RoCoF estimation. In addition, the inflection point detector techniques and PI filter are also new methods that have been developed in recent years; the former skillfully uses the second derivative of frequency to change the characteristics of its symbol and realize the accurate estimation of RoCoF, while the latter can also realize the accurate estimation by choosing appropriate parameters.

5. Conclusions

In low-inertia power systems, the magnitude of the RoCoF can be a crucial index to present the frequency security and stability of the system. Meanwhile, real-time RoCoF tracking can be a key foundation for the development of advanced control and protection techniques in the low-inertia system. This paper discusses the basic concept and estimation techniques of power system RoCoFs. A comprehensive review on the estimation and prediction methods of maximal RoCoF following a contingency and the real-time RoCoF tracking techniques is provided. The review indicates that with the lack of inertia gradually becoming a common and increasingly more severe issue for power systems around the world, the research related to the analysis and estimation of the power system RoCoF can be increasingly more important. Several potential research topics in related fields are provided; the conclusions are as follows:

(i) Grid codes and standards for RoCoF: With the increasingly high penetration of IBRs and the diversified inertia support in the future power system including both the rotational and virtual inertia, the setting of security threshold for the RoCoF will be further studied in order to protect the in-grid devices and avoid potential cascading failure.

(ii) AI techniques for the RoCoF prediction of the power system: The wide application of synchrophasors that can record the dynamic frequency and corresponding RoCoF ensures the rich source of training datum for AI techniques to assess the frequency security and stability of power systems. According to the review, several studies have already been concerned with predicting the maximal RoCoF following the potential contingency of the system, and further research on AI techniques is needed in the future to solve the problem of poor robustness and interpretability of AI techniques. We can expect further development on this topic with the rapid development of AI techniques.

(iii) Real-time RoCoF tracking algorithm with increased accuracy and reliability: Although the existing real-time RoCoF tracking algorithms embedded into the synchrophasor perform a relatively satisfied accuracy, the errors can be induced due to reasons such as the phase jump following a fault. These errors may result in an unexcepted fatal issue for the power system if the obtained RoCoF is fed to the control or protection. Therefore, further research on RoCoF estimation is needed in the future, so as to further improve the accuracy and robustness of RoCoF estimation through the fusion of multiple algorithms.

Author Contributions: Conceptualization, X.D. and R.M.; methodology X.D. and M.L.; resources R.M., P.W. and D.N.; writing-original draft preparation X.D.; writing-review and editing X.D. and J.C.; supervision M.L. All authors have read and agreed to the published version of the manuscript.

Data Availability Statement: Not applicable.

References

1. Kroposki, B.; Johnson, B.; Zhang, Y.C.; Gevorgian, V.; Denholm, P.; Hodge, B.M.; Hannegan, B. Achieving a 100% Renewable Grid: Operating Electric Power Systems with Extremely High Levels of Variable Renewable Energy. *IEEE Power Energy Mag.* **2017**, *15*, 61–73. [CrossRef]
2. Liu, M.Y.; Chen, J.R.; Xie, Y.S.; Deng, X.Y.; Milano, F. Least Square Method for the Identification of Equivalent Inertia Constant. In Proceedings of the 2022 IEEE Power & Energy Society General Meeting (PESGM), Denver, CO, USA, 17–21 July 2022.
3. Milano, F.; Dörfler, F.; Hug, G.; Hill, D.J.; Verbič, G. Foundations and Challenges of Low-Inertia Systems (Invited Paper). In Proceedings of the 2018 Power Systems Computation Conference (PSCC), Dublin, Ireland, 11–15 June 2018.
4. Winter, W.; Elkington, K.; Bareux, G.; Kostevc, J. Pushing the Limits: Europe's New Grid: Innovative Tools to Combat Transmission Bottlenecks and Reduced Inertia. *IEEE Power Energy Mag.* **2015**, *13*, 60–74. [CrossRef]
5. Panda, R.K.; Mohapatra, A.; Srivastava, S.C. Application of Indirect Adaptive Control Philosophy for Inertia Estimation. In Proceedings of the 2019 IEEE PES GTD Grand International Conference and Exposition Asia (GTD Asia), Bangkok, Thailand, 19–23 March 2019.
6. Mo, R.; Deng, X.Y.; Liu, M.Y.; Chang, X.Q. Ambient-Measurement-Based Equivalent Inertia Constant Identification Via Tikhonov Regularization Algorithm. In Proceedings of the 2022 International Conference on Renewable Energies and Smart Technologies (REST), Tirana, Albania, 28–29 July 2022.
7. Nedd, M.; Browell, J.; Bell, K.; Booth, C. Containing a Credible Loss to Within Frequency Stability Limits in a Low-Inertia GB Power System. *IEEE Trans. Ind. Appl.* **2020**, *56*, 1031–1039. [CrossRef]
8. Pandey, A.; Kumar, S.; Mohire, S.; Pentayya, P.; Kazi, F. Dynamic Modeling and Cascade Failure Analysis of the Mumbai Grid Incident of October 12, 2020. *IEEE Access* **2022**, *10*, 43598–43610. [CrossRef]
9. Frigo, G.; Derviškadić, A.; Zuo, Y.H.; Paolone, M. PMU-Based ROCOF Measurements: Uncertainty Limits and Metrological Significance in Power System Applications. *IEEE Trans. Instrum. Meas.* **2019**, *68*, 3810–3822. [CrossRef]
10. Albu, M.; Dumitrescu, A.M.; Popovici, R. Rate of change of frequency—A power quality descriptor. In Proceedings of the 2014 16th International Conference on Harmonics and Quality of Power (ICHQP), Bucharest, Romania, 25–28 May 2014.
11. Milano, F.; Ortega, Á. A Method for Evaluating Frequency Regulation in an Electrical Grid-Part I: Theory. *IEEE Trans. Power Syst.* **2021**, *36*, 183–193. [CrossRef]
12. Ortega, Á.; Milano, F. A Method for Evaluating Frequency Regulation in an Electrical Grid-Part II: Applications to Non-Synchronous Devices. *IEEE Trans. Power Syst.* **2021**, *36*, 194–203. [CrossRef]
13. Zhao, J.B.; Mili, L.; Milano, F. Robust Frequency Divider for Power System Online Monitoring and Control. *Trans. Power Syst.* **2018**, *33*, 4414–4423. [CrossRef]
14. Zhao, R.Z.; Wen, Y.F.; Ye, X.; Tang, Q.; Li, W.Y.; Chen, Y.H.; Qu, X.B. Research on Frequency Indicators Evaluation of Disturbance Events Based on Improved Stacked Denoising Autoencoders. *Proc. CSEE* **2019**, *39*, 4081–4093.
15. Wen, Y.F.; Zhao, R.Z.; Xiao, Y.Q.; Liu, Z.B. Power system frequency stability assessment based on multi-layer extreme learning machine. *Autom. Electr. Power Syst.* **2019**, *43*, 133–143.
16. Hu, Y.L.; Wei, W.; Peng, Y.G.; Lei, J.Y. Fuzzy virtual inertia control for virtual synchronous generator. In Proceedings of the 35th Chinese Control Conference, Chengdu, China, 27–29 July 2016.
17. Maaruf, M.; Ferik, S.E.; Al-Ismail, F.S.; Khalid, M. Robust Optimal Virtual Inertia Control for Microgrid Frequency Regulation Considering High Renewable Energy Penetration. In Proceedings of the 1st IEEE International Conference on Renewable Energy Research and Applications, Istanbul, Turkey, 18–21 September 2022.
18. Gupta, P.; Bhatia, R.S.; Jain, D.K. Active ROCOF Relay for Islanding Detection. *IEEE Trans. Power Deliver.* **2017**, *32*, 420–429. [CrossRef]
19. Alam, M.R.; Begum, M.T.A.; Muttaqi, K.M. Assessing the Performance of ROCOF Relay for Anti-Islanding Protection of Distributed Generation Under Subcritical Region of Power Imbalance. *IEEE Trans. Ind. Appl.* **2019**, *55*, 5395–5405. [CrossRef]
20. *IEEE Std C37.118^{TM}.1-2011 (Revision of IEEE Std C37.118^{TM}-2005)*; IEEE Standard for Synchrophasor Measurements for Power Systems. IEEE Power & Energy Society: Piscataway, NJ, USA, 2011; pp. 1–61.
21. Wang, M.H.; Sun, Y.Z. A practical method to improve phasor and power measurement accuracy of DFT algorithm. *IEEE Trans. Power Deliver.* **2006**, *21*, 1054–1062. [CrossRef]
22. Yang, R.G.; Xue, H. A Novel Algorithm for Accurate Frequency Measurement Using Transformed Consecutive Points of DFT. *IEEE Trans. Power Syst.* **2008**, *23*, 1057–1062. [CrossRef]
23. Castello, P.; Liu, J.Q.; Muscas, C.; Pegoraro, P.A.; Ponci, F.; Monti, A. A Fast and Accurate PMU Algorithm for P+M Class Measurement of Synchrophasor and Frequency. *IEEE Trans. Instrum. Meas.* **2014**, *63*, 2837–2845. [CrossRef]
24. Wright, P.S.; Davis, P.N.; Johnstone, K.; Rietveld, G.; Roscoe, A.J. Field Measurement of Frequency and ROCOF in the Presence of Phase Steps. *IEEE Trans. Instrum. Meas.* **2019**, *68*, 1688–1695. [CrossRef]
25. Roscoe, A.J.; Dyśko, A.; Marshall, B.; Lee, M.; Kirkham, H.; Rietveld, G. The Case for Redefinition of Frequency and ROCOF to Account for AC Power System Phase Steps. In Proceedings of the 2017 IEEE International Workshop on Applied Measurements for Power Systems (AMPS), Liverpool, UK, 20–22 September 2017.
26. Li, T.; Li, Y.; Li, S.; Zhang, W. Research on Current-Limiting Control Strategy Suitable for Ground Faults in AC Microgrid. *IEEE J. Emerg. Sel. Top. Power* **2021**, *9*, 1736–1750. [CrossRef]

27. Masood, N.A.; Yan, R.F.; Saha, T.K. Cascading Contingencies in a Renewable Dominated Power System: Risk of Blackouts and Its Mitigation. In Proceedings of the 2018 IEEE Power & Energy Society General Meeting (PESGM), Portland, OR, USA, 5–10 August 2018.

28. Jamborsalamati, P.; Moghimi, M.; Hossain, M.J.; Taghizadeh, S.; Lu, J.; Konstantinou, G. A Framework for Evaluation of Power Grid Resilience Case Study: 2016 South Australian Blackout. In Proceedings of the 2018 IEEE International Conference on Environment and Electrical Engineering and 2018 IEEE Industrial and Commercial Power Systems Europe (EEEIC/I&CPS Europe), Palermo, Italy, 12–15 June 2018.

29. Yan, R.F.; Masood, N.A.; Saha, T.K.; Bai, F.F.; Gu, H.J. The Anatomy of the 2016 South Australia Blackout: A Catastrophic Event in a High Renewable Network. *IEEE Trans. Power Syst.* **2018**, *33*, 5374–5388. [CrossRef]

30. Lai, L.L.; Zhang, H.T.; Mishra, S.; Ramasubramanian, D.; Lai, C.S.; Xu, F.Y. Lessons learned from July 2012 Indian blackout. In Proceedings of the 9th IET International Conference on Advances in Power System Control, Operation and Management (APSCOM 2012), Hong Kong, China, 18–21 November 2012.

31. Rampurkar, V.; Pentayya, P.; Mangalvedekar, H.A.; Kazi, F. Cascading Failure Analysis for Indian Power Grid. *IEEE Trans. Smart Grid* **2016**, *7*, 1951–1960. [CrossRef]

32. Suresh, V.; Sutradhar, R.; Mandal, S.; Debnath, K. Near Miss of Blackout in Southern Part of North Eastern Grid of India. In Proceedings of the 2020 3rd International Conference on Energy, Power and Environment: Towards Clean Energy Technologies, Shillong, Meghalaya, India, 5–7 March 2021.

33. Hartono, J.; Pramana, P.A.A.; Kusuma, A.A.; Munir, B.S. Power System Inertia Estimation Based on Frequency Measurement. In Proceedings of the 2019 Asia Pacific Conference on Research in Industrial and Systems Engineering (APCoRISE), Depok, Indonesia, 18–19 April 2019.

34. Liu, M.Y.; Chen, J.R.; Milano, F. On-Line Inertia Estimation for Synchronous and Non-Synchronous Devices. *IEEE Trans. Power Syst.* **2021**, *36*, 2693–2701. [CrossRef]

35. Delkhosh, H.; Seifi, H. Power System Frequency Security Index Considering All Aspects of Frequency Profile. *IEEE Trans. Power Syst.* **2021**, *36*, 1656–1659. [CrossRef]

36. Sun, M.; Xie, G.W.; Chen, L.; Liu, Y.M.; Li, X.J.; Min, Y. Study on the Necessity and Role of Inertia in Power System Frequency Response. In Proceedings of the 2020 IEEE 4th Conference on Energy Internet and Energy System Integration (EI2), Wuhan, China, 30 October–1 November 2020.

37. Bevrani, H.; Golpîra, H.; Messina, A.R.; Hatziargyriou, N.; Milano, F.; Ise, T. Power system frequency control: An updated review of current solutions and new challenges. *Electr. Power Syst. Res.* **2021**, *194*, 107114. [CrossRef]

38. Kundur, P. *Power System Stability and Control*; McGraw-Hill: New York, NY, USA, 1994.

39. Tan, B.D.; Zhao, J.B.; Netto, M.; Krishnan, V.; Terzija, V.; Zhang, Y.C. Power System Inertia Estimation: Review of Methods and the Impacts of Converter-Interfaced Generations. *Int. J. Elec. Power* **2022**, *134*, 107362. [CrossRef]

40. Hatziargyriou, N.; Rahmann, C.; Canizares, C.; Hiskens, I.; Pourbeik, P.; Cutsem, T.V. Definition and Classification of Power System Stability–Revisited & Extended. *IEEE Trans. Power Syst.* **2021**, *36*, 3271–3281.

41. Wen, J.X.; Bu, S.Q.; Li, F.X.; Du, P.W. Risk assessment and mitigation on area-level RoCoF for operational planning. *Energy* **2021**, *228*, 120632. [CrossRef]

42. Zhao, J.B.; Tang, Y.; Terzija, V. Robust Online Estimation of Power System Center of Inertia Frequency. *IEEE Trans. Power Syst.* **2019**, *34*, 821–825. [CrossRef]

43. Milano, F.; Ortega, Á. Frequency divider. *IEEE Trans. Power Syst.* **2017**, *32*, 1493–1501.

44. Ortega, Á.; Milano, F. Frequency Participation Factors. *IEEE Trans. Power Syst.* **2018**, *33*, 5563–5571. [CrossRef]

45. Wen, J.X.; Bu, S.Q.; Zhou, B.W.; Chen, Q.Y.; Yang, H.K. A Fast-Algorithmic Probabilistic Evaluation on Regional Rate of Change of Frequency (RoCoF) for Operational Planning of High Renewable Penetrated Power Systems. *Energies* **2020**, *13*, 2780. [CrossRef]

46. Milano, F. Rotor Speed-Free Estimation of the Frequency of the Center of Inertia. *IEEE Trans. Power Syst.* **2018**, *33*, 1153–1155. [CrossRef]

47. Sauer, P.W.; Pai, M.A. *Power System Dynamics and Stability*; Prentice Hall: Upper Saddle River, NJ, USA, 1998.

48. Milano, F. *Power System Modelling and Scripting*; Springer: London, UK, 2010.

49. Bašakarad, T.; Holjevac, N.; Kuzle, I.; Ivanković, I.; Zovko, N. Rocof Importance in Electric Power Systems with High Renewables Share: A Simulation Case for Croatia. In Proceedings of the 12th Mediterranean Conference on Power Generation, Transmission, Distribution and Energy Conversion (MEDPOWER 2020), Online Conference, 9–12 November 2020.

50. Doheny, D.; Conlon, M. Investigation into the local nature of rate of change of frequency in electrical power systems. In Proceedings of the 2017 52nd International Universities Power Engineering Conference (UPEC), Heraklion, Greece, 28–31 August 2017.

51. Ghosh, R.; Tummuru, N.R.; Rajpurohit, B.S.; Monti, A. Virtual Inertia from Renewable Energy Sources: Mathematical Representation and Control Strategy. In Proceedings of the 2020 IEEE International Conference on Power Electronics, Smart Grid and Renewable Energy (PESGRE2020), Cochin, India, 2–4 January 2020.

52. Inoue, T.; Taniguchi, H.; Ikeguchi, Y.; Yoshida, K. Estimation of power system inertia constant and capacity of spinning-reserve support generators using measured frequency transients. *IEEE Trans. Power Syst.* **1997**, *12*, 136–143. [CrossRef]

53. Du, P.W.; Makarov, Y. Using Disturbance Data to Monitor Primary Frequency Response for Power System Interconnections. *IEEE Trans. Power Syst.* **2014**, *29*, 1431–1432. [CrossRef]

54. Phurailatpam, C.; Rather, Z.H.; Bahrani, B.; Doolla, S. Measurement-Based Estimation of Inertia in AC Microgrids. *IEEE Trans. Sustain. Energ.* **2020**, *11*, 1975–1984. [CrossRef]

55. *IEEE Std C37.118.1a™-2014 (Amendment to IEEE Std C37.118.1™-2011)*; IEEE Standard for Synchrophasor Measurements for Power Systems. IEEE Power & Energy Society: Piscataway, NJ, USA, 2014; pp. 1–25.

56. Bründlinger, R. *Grid Codes in Europe—Overview on the Current Requirements in European Codes and National Interconnection Standards*; AIT Austrian Institute of Technology: Vienna, Austria, 2019.

57. DGA Consulting. International Review of Frequency Control Adaptation. *Australian Energy Market Operator*, 14 October 2016.

58. Khalili, S.; Breyer, C. Review on 100% Renewable Energy System Analyses—A Bibliometric Perspective. *IEEE Access* **2022**, *10*, 125792–125834. [CrossRef]

59. Jacobson, M.Z.; Krauland, A.K.V.; Burton, Z.F.M.; Coughlin, S.J.; Jaeggli, C.; Nelli, D.; Nelson, A.J.H.; Shu, Y.B.; Smith, M.; Tan, C.; et al. Transitioning All Energy in 74 Metropolitan Areas, Including 30 Megacities, to 100% Clean and Renewable Wind, Water, and Sunlight (WWS). *Energies* **2020**, *13*, 4934. [CrossRef]

60. Roy, N.K.; Islam, S.; Podder, A.K.; Roy, T.K.; Muyyen, S.M. Virtual Inertia Support in Power Systems for High Penetration of Renewables—Overview of Categorization, Comparison, and Evaluation of Control Techniques. *IEEE Access* **2022**, *10*, 129190–129216. [CrossRef]

61. Zaid, S.A.; Bakeer, A.; Magdy, G.; Albalawi, H.; Kassem, A.M.; El-Shimy, M.E.; AbdelMeguid, H.; Manqarah, B. A New Intelligent Fractional-Order Load Frequency Control for Interconnected Modern Power Systems with Virtual Inertia Control. *Fractal Fract.* **2023**, *7*, 62. [CrossRef]

62. Wang, T.; Jin, M.X.; Li, Y.D.; Wang, J.M.; Wang, Z.P.; Huang, S.L. Adaptive Damping Control Scheme for Wind Grid-Connected Power Systems with Virtual Inertia Control. *IEEE Trans. Power Syst.* **2022**, *37*, 3902–3912. [CrossRef]

63. *IEC/IEEE 60255-118-1*; IEEE/IEC International Standard–Measuring Relays and Protection Equipment–Part 118-1: Synchrophasor for Power Systems–Measurements. IEEE: Piscataway, NJ, USA, 2018; pp. 1–78.

64. Sozanski, K.; Szczesniak, P. Advanced Control Algorithm for Three-Phase Shunt Active Power Filter Using Sliding DFT. *Energies* **2023**, *16*, 1453. [CrossRef]

65. Bertocco, M.; Frigo, G.; Narduzzi, C.; Muscas, C.; Pegoraro, P.A. Compressive Sensing of a Taylor–Fourier Multifrequency Model for Synchrophasor Estimation. *IEEE Trans. Instrum. Meas.* **2015**, *64*, 3274–3283. [CrossRef]

66. Grandke, T. Interpolation Algorithms for Discrete Fourier Transforms of Weighted Signals. *IEEE Trans. Instrum.* **1983**, *32*, 350–355. [CrossRef]

67. Belega, D.; Petri, D. Accuracy Analysis of the Multicycle Synchrophasor Estimator Provided by the Interpolated DFT Algorithm. *IEEE Trans. Instrum. Meas.* **2013**, *62*, 942–953. [CrossRef]

68. Li, Z.Q.; Zhang, W.F.; Zhuang, Z.Y.; Jin, T. A Novel Synchrophasor Estimation Based on Enhanced All-Phase DFT with Iterative Compensation and Its Implementation. *Energies* **2022**, *15*, 6964. [CrossRef]

69. Xu, C.J.; Zhou, L.Y.; Chen, C.; Zhang, Q.Y. A Low Computational Complexity Frequency Estimation Method with High Precision of Sinusoid Based on DFT. In Proceedings of the 2017 4th International Conference on Information Science and Control Engineering (ICISCE), Changsha, China, 21–23 July 2017.

70. Castello, P.; Ferrero, R.; Pegoraro, P.A.; Toscani, S. Space Vector Taylor–Fourier Models for Synchrophasor, Frequency, and ROCOF Measurements in Three-Phase Systems. *IEEE Trans. Instrum. Meas.* **2019**, *68*, 1313–1321. [CrossRef]

71. Petri, D.; Fontanelli, D.; Macii, D.; Belega, D. A DFT-based synchrophasor, frequency and ROCOF estimation algorithm. In Proceedings of the 2013 IEEE International Workshop on Applied Measurements for Power Systems (AMPS), Aachen, Germany, 25–27 September 2013.

72. Romano, P.; Paolone, M. Enhanced Interpolated-DFT for Synchrophasor Estimation in FPGAs: Theory, Implementation, and Validation of a PMU Prototype. *IEEE Trans. Instrum. Meas.* **2014**, *63*, 2824–2836. [CrossRef]

73. Jain, V.K.; Collins, W.L.; Davis, D.C. High-Accuracy Analog Measurements via Interpolated FFT. *IEEE Trans. Instrum. Meas.* **1979**, *28*, 113–122. [CrossRef]

74. Belega, D.; Macii, D.; Petri, D. Fast Synchrophasor Estimation by Means of Frequency-Domain and Time-Domain Algorithms. *IEEE Trans. Instrum. Meas.* **2014**, *63*, 388–401. [CrossRef]

75. Andria, G.; Savino, M.; Trotta, A. Windows and interpolation algorithms to improve electrical measurement accuracy. *IEEE Trans. Instrum. Meas.* **1989**, *38*, 856–863. [CrossRef]

76. Derviškadić, A.; Romano, P.; Paolone, M. Iterative-interpolated DFT for synchrophasor estimation in M-class compliant PMUs. In Proceedings of the 2017 IEEE Manchester PowerTech, Manchester, UK, 18–22 June 2017.

77. Wu, X.H.; Qian, Q.Q.; Bao, Y.Q. Demand Response Using Disturbance Estimation-Based Kalman Filtering for the Frequency Control. *Energies* **2022**, *15*, 9377. [CrossRef]

78. Namba, M.; Nishiwaki, T.; Yokokawa, S.; Ohtsuka, K.; Ueki, Y. Identification of Parameters for Power System Stability Analysis Using Kalman Filter. *IEEE Trans. Power Appar. Syst.* **1981**, *PER-1*, 37. [CrossRef]

79. Huang, C.H.; Lee, C.H.; Shih, K.J.; Wang, Y.J. Frequency Estimation of Distorted Power System Signals Using a Robust Algorithm. *IEEE Trans. Power Deliver.* **2008**, *23*, 41–51. [CrossRef]

80. Wu, C.C.; Magaña, M.E.; Cotilla-Sánchez, E. Dynamic Frequency and Amplitude Estimation for Three-Phase Unbalanced Power Systems Using the Unscented Kalman Filter. *IEEE Trans. Instrum. Meas.* **2019**, *68*, 3387–3395. [CrossRef]

81. Wan, W.K.; Feng, J.G.; Song, B.; Li, X.X. Huber-Based Robust Unscented Kalman Filter Distributed Drive Electric Vehicle State Observation. *Energies* **2021**, *14*, 750. [CrossRef]
82. Fontanelli, D.; Macii, D.; Petri, D. Dynamic synchrophasor estimation using Smoothed Kalman filtering. In Proceedings of the 2016 IEEE International Instrumentation and Measurement Technology Conference Proceedings, Taipei, Taiwan, 23–26 May 2016.
83. Gajjar, G.; Soman, S.A. Auto detection of power system events using wide area frequency measurements. In Proceedings of the 2014 Eighteenth National Power Systems Conference (NPSC), Guwahati, India, 18–20 December 2014.
84. Shaw, P.; Jena, K.M. A Novel Event Detection and Classification Scheme Using Wide-Area Frequency Measurements. *IEEE Trans. Smart Grid* **2021**, *12*, 2320–2330. [CrossRef]
85. Wilches-Bernal, F.; Wold, J.; Concepcion, R.; Budai, J. A Method for Correcting Frequency and RoCoF Estimates of Power System Signals with Phase Steps. In Proceedings of the 2019 North American Power Symposium (NAPS), Wichita, KS, USA, 13–15 October 2019.
86. Szabat, K.; Wróbel, K.; Dróżdż, K.; Janiszewski, D.; Pajchrowski, T.; Wójcik, A. A Fuzzy Unscented Kalman Filter in the Adaptive Control System of a Drive System with a Flexible Joint. *Energies* **2020**, *13*, 2056. [CrossRef]
87. Qi, J.J.; Sun, K.; Wang, J.H.; Liu, H. Dynamic State Estimation for Multi-Machine Power System by Unscented Kalman Filter with Enhanced Numerical Stability. *IEEE Trans. Smart Grid* **2018**, *9*, 1184–1196. [CrossRef]
88. Gao, C.; Sun, J. Dynamic State Estimation for Power System Based on M-UKF Algorithm. In Proceedings of the 2020 IEEE 4th Conference on Energy Internet and Energy System Integration (EI2), Wuhan, China, 30 October 2020–1 November 2020.
89. Zhao, H.Q.; Tian, B.Y. Robust Power System Forecasting-Aided State Estimation with Generalized Maximum Mixture Correntropy Unscented Kalman Filter. *IEEE Trans. Instrum. Meas.* **2022**, *71*, 9002610. [CrossRef]
90. Singh, A.K.; Pal, B.C. Rate of Change of Frequency Estimation for Power Systems Using Interpolated DFT and Kalman Filter. *IEEE Trans. Power Syst.* **2019**, *34*, 2509–2517. [CrossRef]
91. Ghahremani, E.; Kamwa, I. Online State Estimation of a Synchronous Generator Using Unscented Kalman Filter from Phasor Measurements Units. *IEEE Trans. Energy Conver.* **2011**, *26*, 1099–1108. [CrossRef]
92. Wang, S.B.; Gao, W.Z.; Meliopoulos, A.P.S. An Alternative Method for Power System Dynamic State Estimation Based on Unscented Transform. *IEEE Trans. Power Syst.* **2012**, *27*, 942–950. [CrossRef]
93. Karimi, H.; Karimi-Ghartemani, M.; Iravani, M.R. Estimation of frequency and its rate of change for applications in power systems. *IEEE Trans. Power Deliver.* **2004**, *19*, 472–480. [CrossRef]
94. Toscani, S.; Muscas, C.; Pegoraro, P.A. Design and Performance Prediction of Space Vector-Based PMU Algorithms. *IEEE Trans. Instrum. Meas.* **2017**, *66*, 394–404. [CrossRef]
95. Ferrero, R.; Pegoraro, P.A.; Toscani, S. A Space Vector Phase-Locked-Loop Approach to Synchrophasor, Frequency and Rocof Estimation. In Proceedings of the 2019 IEEE International Instrumentation and Measurement Technology Conference (I2MTC), Auckland, New Zealand, 20–23 May 2019.
96. Yao, W.X.; You, S.T.; Wang, W.K.; Deng, X.D.; Li, Y.C.; Zhan, L.W.; Liu, Y.L. A Fast Load Control System Based on Mobile Distribution-Level Phasor Measurement Unit. *IEEE Trans. Smart Grid* **2020**, *11*, 895–904. [CrossRef]
97. Yin, H.; Wu, Y.R.; Qiu, W.; Zeng, C.J.; You, S.T.; Tan, J.; Hoke, J.; Kruse, C.J.; Rockwell, B.W.; Kawamura, K.A.; et al. Precise ROCOF estimation algorithm for low inertia power grids. *Electr. Pow. Syst. Res.* **2022**, *209*, 107968. [CrossRef]
98. Belega, D.; Fontanelli, D.; Petri, D. Dynamic Phasor and Frequency Measurements by an Improved Taylor Weighted Least Squares Algorithm. *IEEE Trans. Instrum. Meas.* **2015**, *64*, 2165–2178. [CrossRef]
99. Sun, M.Y.; Liu, G.Y.; Popov, M.; Terzija, V. Azizi, S. Underfrequency Load Shedding Using Locally Estimated RoCoF of the Center of Inertia. *IEEE Trans. Power Syst.* **2021**, *36*, 4212–4222. [CrossRef]
100. You, S.T.; Li, H.Y.; Liu, S.Y.; Sun, K.Q.; Wang, W.K.; Liu, Y.L. Calculate Center-of-Inertia Frequency and System RoCoF Using PMU Data. In Proceedings of the 2021 IEEE Power & Energy Society General Meeting (PESGM), Washington, DC, USA, 26–29 July 2021.